# Photodegradation of Perfluorooctanesulfonic Acid on Fe-Zeolites in Water

*Lin Qian, Frank-Dieter Kopinke and Anett Georgi**

Department of Environmental Engineering, Helmholtz Centre for Environmental Research – UFZ, Permoserstrasse 15, D-04318 Leipzig, Germany

**ABSTRACT:** Perfluorooctanesulfonic acid (PFOS) decomposition in an aqueous environment remains a huge challenge because of its extreme chemical and biological inertness even when compared with other per- and polyfluoroalkyl substances (PFAS). In this work, we demonstrate for the first time a successful photochemical PFOS degradation by irradiation with 254 nm ultraviolet (UV) light after adsorption on μm-sized Fe(III)-loaded zeolites under ambient conditions with oxygen ($O_2$) as the terminal oxidant. 20 μM PFOS loaded on 0.5 g $L^{-1}$ Fe-zeolites in aqueous suspension was degraded up to 99% within 96 h under acidic conditions (pH ≤ 5.5) in the presence of oxygen. Besides fluoride and sulfate, short-chain perfluorinated carboxylic acids (PFCAs) were identified and quantified as products. In addition, the effects of initial pH, catalyst dosages, and operation temperature on the degradation of PFOS were investigated. We also successfully applied the system to real groundwater samples where trace PFOS was present. Our results indicate that PFOS degradation is initiated by electron transfer from sulfonate to iron. The

presented experimental study offers an option for a novel water remediation technology, comprising first a zeolite-based adsorption step followed by a step for photochemical regeneration of the adsorbent.

## 1. Introduction

Perfluorooctanesulfonic acid (PFOS) is one of the most important per- and polyfluoroalkyl substances (PFAS) being widely used in manufacturing industrial and consumer products,[1] such as fire retardants, high-temperature lubricants, waterproof textiles, and Teflon-related products.[2] PFOS has been found to be globally distributed in aquatic and terrestrial environments[3] and also in many organisms.[4, 5] Several studies suggest that the exposure to PFOS over certain levels may result in harmful health effects in humans and animals, i.e. liver and kidney toxicity, cardiotoxicity, reproductive toxicity and neurotoxicity.[6-9] Even though production and use of the extremely persistent PFOS was phased out after the compound was added to Annex B of the Stockholm Convention, the risk of human exposure due to accumulation in marine systems and contaminations in groundwater used for drinking water production will continue to exist for decades.[10]

PFOS is resistant to most of the conventional reduction/oxidation processes and biological degradation due to its strong C-F bonds.[11] Advanced oxidation processes (AOPs) are ineffective as PFAS have negligible reactivity with hydroxyl radicals,[12] the main reactant in AOPs.[13] Destruction of perfluorinated *carboxylic* acids (PFCAs) was achieved in persulfate systems activated by heat or UV irradiation, but PFOS was found inert to such approaches.[14] Although there is substantial published research on the degradation of PFCAs, e.g., perfluorooctanoic acid (PFOA), studies on the degradation of PFOS remain rather limited. The reason is that degradation of PFOS is an even greater challenge than that of PFCAs.

There are two major approaches reported to be effective in the degradation of PFOS. First, the reductive pathway using hydrated electrons ($e_{aq}^-$) as reactive species, generated by UV photolysis of potassium iodide,[15] sodium sulfite,[16] or indole acetic acid.[17] However, the generation of hydrated electrons requires alkaline and anaerobic conditions, and furthermore, the produced byproducts have the potential to contaminate the treated water. Alternatively, PFOS can be degraded electrochemically, e.g. at boron-doped diamond (BDD) electrodes. It has been reported that the oxidation of PFOS is initiated by direct electron transfer from PFOS to the anode,[18] after which a sequence of radical and hydrolysis reactions can take place. However, a significant shortcoming of this process is its low space-time-yield, in particular for highly diluted water fluxes.[18] In summary, there is an urgent need to develop a method for decomposing PFOS ecologically and economically under feasible and practically available conditions.

Nowadays, UV irradiation is becoming more and more widespread as a method for disinfecting drinking, waste, and feed waters.[19] Unfortunately, PFOS has almost no absorbance in the UV range and cannot be directly photolyzed by UV light.[20] This obstacle can be overcome using coordination complexes which interact with photons of artificial UV or solar light giving rise to their photodecomposition. For instance, it has been reported that PFOS can be complexed with ferric ions to form $[PFOS\text{-}Fe]^{2+}$ (eq 1). The complex can be excited under vacuum-ultraviolet (VUV, 185 nm) or ultraviolet-C (UV-C, 254 nm) irradiation to produce ferrous ions and $C_8F_{17}SO_3\cdot$ via ligand-to-metal electron transfer (eq 2).[21]

$$C_8F_{17}SO_3^- + Fe^{3+} \longleftrightarrow [C_8F_{17}SO_3\text{-}Fe]^{2+} \quad (1)$$

$$[C_8F_{17}SO_3\text{-}Fe]^{2+} \xrightarrow{\text{UV- C}} C_8F_{17}SO_3\cdot + Fe^{2+} \quad (2)$$

Desulfurization of $C_8F_{17}SO_3\cdot$ yields perfluorinated alkyl radicals, which may react with oxygen or hydroxyl radicals to be further decomposed. However, the shortcomings of this ferric-ion-

mediated photodecomposition of PFOS in homogeneous systems are obvious: (i) the operational pH range is restricted to pH ≤ 3, (ii) reaction rates are low, and (iii) the reaction is probably vulnerable to the real water matrix[22] so an additional pre-enrichment of PFOS is desirable.

In the present study, a complementary combination of efficient PFOS adsorption on commercially available µm-sized Fe(III)-loaded BEA-type zeolite particles (Fe-BEA35, details see the SI) and photo-oxidation under UV-C irradiation is proposed. This overcomes several issues of the existing PFOS degradation techniques. The Fe-BEA35 zeolite was characterized in detail and first applied for photochemical degradation of PFOA using UV-A light in our previous study.[23] Nevertheless, PFOS is known as more persistent than perfluorocarboxylic acids as it is, e.g., unreactive in e-transfer by sulfate radicals. In this study we show for the first time that PFOS is degraded using these microscale Fe-zeolite particles when irradiated with UV-C light and identify the operation steps and conditions for its complete mineralization. Thanks to the high adsorption affinity toward PFOS, Fe-BEA35 can act as an efficient adsorbent for this contaminant, whereby the ferric ions embedded in the zeolites possess desirable coordination and catalytic abilities while being much less vulnerable to the surrounding water matrix. Furthermore, the effects of pH, zeolite dosages, and operation temperature on degradation of PFOS are investigated in this work. Our study shows for the first time that this heterogeneous system works successfully in real groundwater. Furthermore, it can be operated in a wider pH range (up to pH 5.5) than the homogeneous process. The findings in this study offer a promising new strategy for remediation of water containing low concentrations of PFOS.

## 2. Experimental Section

Detailed information on chemicals, materials, photochemical procedures, and analyses is described in the Supporting Information (SI). For a typical photochemical PFOS degradation, a

350-mL reaction suspension containing certain amounts of Fe-zeolites and PFOS was loaded in a closed-system reactor. A low-pressure mercury lamp (254 nm, 20 W) was used for all reactions. Details about the reactor setup and the groundwater sample treatment are shown in Figures S1 and S2. In this study, the desulfurization ratio ($d_{SO_4^{2-}}$) and defluorination ratio ($d_{F^-}$) are calculated as follows:

$$d_{SO_4^{2-}} = \frac{C_{SO_4^{2-}}}{C_0} \times 100\% \quad (3)$$

$$d_{F^-} = \frac{C_{F^-}}{17 \times C_0} \times 100\% \quad (4)$$

where $C_{SO_4^{2-}}$ is the sulfate concentration (μM), $C_{F^-}$ is the fluoride concentration (μM), and $C_0$ is the initial concentration of PFOS (μM). The factor 17 is the number of fluorine atoms in one PFOS molecule. A complete desulfonation and defluorination of PFOS would yield $d_{SO_4^{2-}}$ and $d_{F^-}$ of 100%, respectively.

## 3. Result and Discussion

**3.1. Degradation of PFOS by UV.** A typical reaction suspension contained 0.5 g $L^{-1}$ Fe-BEA35 and $C_{0,PFOS}$ = 20 μM with initial $pH_0$ = 3.0. Under these conditions, after a 24-h equilibration PFOS was predominantly in the adsorbed state (98%) before start of the irradiation. Thus, the initial loading of PFOS on the zeolite was 19.6 mg $g^{-1}$ (Table S1). In order to follow the total concentration of PFOS (including adsorbed and freely dissolved fraction), an extraction step was performed as described in the SI. After a 96-h UV-C irradiation, up to 99% of total initial PFOS was decomposed with $d_{F^-}$ = 69% and $d_{SO_4^{2-}}$= 99% (Figure 1). In order to reveal the key factor causing the high degradation degree in the system, control experiments under the same conditions with (i) neither Fe-BEA35 nor other iron sources, and (ii) dissolved ferric ions but no zeolites were performed. As shown in Figure 1, only little degradation of PFOS (6%) occurred after a 96-h UV-

C irradiation in the systems in the absence of zeolites and in the absence of iron sources, indicating almost no direct photolysis of PFOS. This is not unexpected, as previous studies confirmed that PFOS exhibits no significant adsorption in the UV-C range.[20] Therefore, significant PFOS degradation due to direct photolysis can be ruled out. In the second control experiment, the PFOS degradation performance in a homogeneous system containing 200 μM dissolved ferric ions at pH 3.0 was tested. It is known that PFOS can form complexes with ferric ions in aqueous solution (PFOS-$Fe^{3+}$), which can then be decomposed under UV-C irradiation and contribute to PFOS degradation.[21] With dissolved ferric ions, 69% of the initial PFOS was decomposed, and $d_{F^-}$ = 18% was achieved within 96 h. The lower PFOS degradation (69% in 96 h vs 92% in 24 h) in the homogeneous system strongly suggests that the presence of Fe-BEA35 was responsible for the high PFOS degradation performance in the heterogeneous system. We assume that the adsorption of PFOS to the zeolite is a precondition for photochemical degradation. The fractions of adsorbed PFOS ($X_{sorb}$) and freely dissolved PFOS ($X_{free}$) can be described as follows:

$$X_{sorb} = 1 - X_{free} \quad (5)$$

$$X_{free} = C_{PFOS,free} / C_{PFOS,total} \quad (6)$$

where $C_{PFOS,free}$ and $C_{PFOS,total}$ are the freely dissolved PFOS and total extractable PFOS concentrations, respectively. Similar to our previous study,[23] it is reasonable to hypothesize the complex formation as a prerequisite for photochemical PFOS degradation according to eq 7 and 8:

$$C_8F_{17}SO_3^- + Fe^{3+}\text{-zeolite} \longleftrightarrow [C_8F_{17}SO_3\text{-}Fe]^{2+}\text{-zeolite} \quad (7)$$

$$[C_8F_{17}SO_3\text{-}Fe]^{2+}\text{-zeolite} \xrightarrow{\text{UV- C}} C_8F_{17}SO_3\cdot + Fe^{2+}\text{-zeolite} \quad (8)$$

Based upon this mechanism, a first-order rate equation can be derived

$$\frac{dC_{PFOS}}{dt} = -k \cdot C_{[C_8F_{17}SO_3\text{-}Fe]^{2+}\text{-zeolite}} = -k \cdot X_{complex} \cdot C_{PFOS,total} = -k_{obs,PFOS} \cdot C_{PFOS,total} \quad (9)$$

where $X_{complex}$ is the fraction of PFOS in reactive complexes. While the overall degree of sorption $X_{sorb}$ is experimentally obtained, $X_{complex}$ cannot be easily determined. Hence, we integrate it in the observable rate coefficient $k_{obs,PFOS} = k \cdot X_{complex}$. The initial reaction period (0 – 24 h) can be well fitted by a first-order kinetics (Figure S3). However, the reaction slows down at high turnover (>92% at $t$ >24 h). The influence of PFOS concentration on the rate coefficients together with possible reasons are discussed in detail in Section 3.3.

In order to understand the PFOS photochemical degradation pathways and underlying mechanisms better, intermediate products were investigated. No sulfur-containing compounds other than PFOS and sulfate were detected, and almost full sulfur mass recovery (98%) was obtained, suggesting that the C-S bond of the PFOS anion was cut and sulfate was subsequently produced. Apart from fluoride and sulfate, seven perfluorinated carboxylic acids (PFCAs) with 2 to 8 carbon atoms (named C2 to C8, respectively) were detected and quantified by LC/MS and IC analysis.

The concentration profiles of the PFOS intermediates along the reaction time are shown in Figure 2 (a). The concentrations of C5, C4, and C3 passed maxima at 6, 24, and 72 h, respectively, and decreased subsequently, while the concentration of C2 increased continuously over the whole reaction time. In addition, the early reaction stages (0 to 6 h) were investigated in more detail (Figure S4). It is worth noting that the concentrations of the initially produced C8, C7, C6, and C5 were relatively low, indicating that the reactivity of carboxylates with longer chains (≥C5) is higher than that of PFOS in the presence of Fe-BEA35. Taking the two C8 compounds, sulfonate vs carboxylate, as an example, two batch experiments were performed containing PFOA and PFOS

separately (Figure S5). By fitting the degradation curves using first-order kinetics (eq 9), around 8 times higher $k_{obs}$ of PFOA than that of PFOS was observed under the same conditions. Overall, the reaction pattern indicates that cleavage of the C-S bond in the PFOS molecule yields PFOA, which is decomposed stepwise toward shorter-chain PFCAs. The possible reason for the continuous increase of C2 is that this very polar compound is not likely to be adsorbed by zeolites but rather to be released from the zeolites instead, as shown in Figure S6 and also discussed in the next section.

Figure 2 (b) shows the fluorine mass balance during the degradation of PFOS. The fluorine sources are grouped into four categories: the remaining PFOS, C5 to C8 PFCAs, C2 to C4 PFCAs, and fluoride. After a 24-h adsorption, a total fluorine (i.e., PFOS) recovery of (94 ± 2)% was achieved by acetonitrile (ACN) extraction (see the SI). The small but significant deficit of (6 ± 2)% points to strong or partially irreversible bonding between Fe-BEA35 and PFOS. After irradiation for 96 h, the final recovery of fluorine in the form of various fluorine-containing products was (92 ± 3)%, which indicates a largely complete PFOS conversion. Nevertheless, the incomplete fluorine mass balance during the reaction (at 6, 24, and 48 h) indicates the following: (i) formation of some undetected fluorine-containing intermediates, which finally were converted to PFCAs and fluoride (at 72 and 96 h), and (ii) formation of some strongly bound intermediates, which cannot be thoroughly extracted but remained reactive. In addition, traces (<0.1% of the converted PFOS) of highly volatile 1H-perfluoroalkanes ($C_nF_{2n+1}H$) were detected in the gas phase (Table S2).

In spite of the almost complete PFOS degradation (99%), $d_{F^-}$ = 69% indicates an only partial mineralization, whereas some short-chain PFCAs survived. This is in accordance with our previous findings on PFOA degradation in the Fe-zeolite/UV system.[23] Shorter-chain PFCAs (≤4 C) show a low adsorption degree at the applied zeolite concentration, i.e. they desorb into the

solution phase instead of being further degraded. To confirm that a complete mineralization of PFOS can finally be obtained, the solution phase of the 96 h UV irradiated Fe-zeolite suspension was further treated by UV activation of sodium persulfate ($Na_2S_2O_8$), which was added in five steps (8.4 mM each) every 2 h. As shown in Figure S7, the remaining short-chain PFCAs were nearly completely decomposed (C2 >93%, C3 and C4 >98% removal degree) after 10 h. A nearly complete defluorination ($d_{F^-}$ = 89%) of PFOS was achieved (Figure S8). To sum up, a complete PFOS degradation and defluorination can be achieved in three steps: (i) in the first step, PFOS is removed from water by adsorption on the separable zeolite adsorbent, (ii) the adsorbed (and thus enriched) PFOS can be photochemically degraded on Fe-zeolites, and the adsorbent is " reactively regenerated", and (iii) in the third step, UV/persulfate is applied in order to generate sulfate radicals ($SO_4^{-}\cdot$), which are nonreactive toward PFOS but are able to degrade the remaining PFCAs.[14] This three-step approach is promising for the treatment of PFOS when aiming at its complete mineralization.

**3.2. Effect of pH on Photochemical Degradation of PFOS.** As discussed above, the addition of Fe-BEA35 can greatly enhance the photochemical degradation of PFOS. For practical wastewater treatment, further influential factors of the water matrix must be considered, e.g., the pH value. Therefore, we investigated the photochemical degradation of PFOS at various initial pH conditions, i.e., $pH_0$ = 3.0, 5.5 and 7.0, as shown in Figure 3 (a), (b), and (c). Compared to pH 5.5 (the native pH value of the 0.5 g $L^{-1}$ zeolite suspension with 20 μM PFOS), degradation rate, defluorination, and desulfurization efficiencies were notably improved at pH 3.0. The $k_{obs,PFOS}$ increased from 0.033 $h^{-1}$ to 0.10 $h^{-1}$, and the half-life was shortened from 21 to 7 h (Table S1). Within a 96-h irradiation, nearly complete PFOS degradation could be achieved at both pH values of 3.0 and 5.5, but a higher $d_{F^-}$ was obtained at pH 3.0 (69%) compared to that at pH 5.5 (56%).

The lower defluorination ratio at pH 5.5 is due to lower reaction rates of the formed PFCA intermediates. Their concentration profile along the reaction time at $pH_0 = 5.5$ is presented in Figure S9. Under these conditions, the concentration of C4 plateaued at $t \geq 72$ h, whereas the concentration of C3 and C2 increased continuously over the whole reaction time. In contrast, at $pH_0 = 3.0$, the concentrations of both C4 and C3 decreased after they passed their maxima (Figure 2(a)). One possible reason for the observed pH effect is that the acidic conditions (pH = 3.0) can promote the adsorption of the PFAS on zeolite, as already observed and discussed in our previous study.[23] Table S1 shows the percentages of the PFOS fraction adsorbed on the zeolite ($X_{sorb}$) at pH 3.0 and pH 5.5, which are 98% and 84%, corresponding to PFOS loadings on the zeolite of 19.6 mg $g^{-1}$ and 16.8 mg $g^{-1}$, respectively. A similar pattern was observed in PFCAs adsorption on zeolite, as shown in Figure S6. At both pH values, decreasing $X_{sorb}$ was found for PFCAs with decreasing chain lengths, but still higher $X_{sorb}$ was achieved at pH 3.0 for all PFCAs. In fact, PFOS is nearly exclusively present in its anionic form under all relevant pH conditions due to its very low $pK_a$ value (<0).[24] It is reasonable to assume that the adsorption of PFOS on zeolites is regulated by the combined effect of hydrophobic interactions between the zeolite surface and the perfluoroalkyl chain and electrostatic interactions.[25-27] The latter comprise interactions of the terminal $R\text{-}SO_3^-$ group, which are repulsive with silanol or $Si\text{-}O\text{-}Al^-$ groups of the zeolite surface and attractive with $Fe^{3+}$ bound to ion-exchange sites of the zeolite. When pH decreases from 5.5 to 3.0, the density of negative surface charges on zeolites causing repulsive interactions is diminished, and adsorption of PFOS is promoted.

When the pH was further increased to 7, the degradation, defluorination, and desulfurization efficiencies were strongly inhibited (Figure 3). However, the adsorption of PFOS on zeolites did not decrease significantly (see Table S1) in the range of pH 5.5 to 7. We therefore relate the

reduced PFOS degradation efficiency at pH 7 to the altered $X_{complex}/X_{sorb}$, i.e., the fraction of complexed (reactive) PFOS related to total adsorbed PFOS on the zeolite. As illustrated in Figure 4, the adsorbed PFOS on Fe-BEA35 can be classified into two categories: the nonspecifically adsorbed PFOS and the complexed PFOS (specifically adsorbed PFOS). Upon irradiation, the sulfonate-to-metal charge transfer takes place on the complexed PFOS with its sulfonic group very close to the ferric ions, whereas this charge transfer is hindered on the nonspecifically adsorbed PFOS due to the larger gap between its sulfonic group and the ferric ions. As ferric ions have a high affinity to hydroxide ions,[28] a lower fraction of the complexed PFOS or a higher nonspecifically adsorbed fraction of PFOS can be expected when pH increases. To sum up, a hampered PFOS photochemical degradation upon pH increase was caused by a decreased fraction of complexed PFOS (PFOS-$Fe^{3+}$) and/or a possibly altered ligand environment at the ferric sites where $OH^-$ ligands replace $H_2O$.

**3.3. Effect of Zeolite Dosage and PFOS Concentration.** When the proportion of the Fe-BEA35 dosage and initial PFOS concentration were kept constant, $k_{obs,PFOS}$ and $d_{F^-}$ both remained nearly the same with Fe-BEA35 dosages from 0.25 g $L^{-1}$ to 1.0 g $L^{-1}$ and initial PFOA concentrations from 10 μM to 40 μM (Figure 5 and Table 1).

With a constant Fe-BEA35 dosage of 0.5 g $L^{-1}$, the $k_{obs,PFOS}$ and $d_{F^-}$ underwent only a minor decrease when the initial PFOS concentration was reduced from 20 μM to 10 μM. However, when considering PFOS concentrations in the range of real contaminated water (46 nM total PFOS, corresponding to $C_{PFOS,free}$ = 0.25 nM), a significant decline in $k_{obs,PFOS}$ was observed, approximately by a factor of 7 (Table 1). In fact, a deceleration of the reaction and 0.4 μM total remaining PFOS was found in the system with initially 20 μM PFOS after a 96-h irradiation, also suggesting that a lower $k_{obs,\ PFOS}$ would appear when low PFOS concentrations are reached. The

possible reason is that even if the Fe-BEA35 dosage is constant and a similar $X_{sorb}$ is achieved at different PFOS concentrations, the PFOS loading on the zeolite ($q_{PFOS}$) is strongly decreased at lower PFOS concentrations, and a much higher single-point sorption coefficient ($K_d = q_{PFOS}/C_{PFOS,free}$) is observed (Table 1). As a result, a lower $X_{complex}/X_{sorb}$ ratio is likely expected with a lower PFOS concentration, due to the increase of some strongly but non-Fe bonded adsorbates (nonspecifically adsorbed PFOS). That is to say, the $X_{complex}/X_{sorb}$ apparently decreases not only with increasing pH (as discussed in Section 3.2) but also at lower PFOS concentrations.

To sum up, increasing the zeolite concentration to a certain extent while keeping the ratio of zeolite dosage to the PFOS initial concentration constant will not influence the reaction rate, making it possible to modify the zeolite concentration for application. The overall reaction rate decreases at a very low initial PFOS concentration. In practice, a preconcentration of PFOS should be provided in order to make the best use of the established Fe-BEA35/UV system with a high PFOS degradation rate.

**3.4. Effect of Operation Temperature.** Increasing temperature would improve chemical reaction rates in most cases, but enhanced temperatures are rarely practical in wastewater treatment due to energy efficiency considerations.[29] Nevertheless, there is a potential to apply photochemical degradation of PFOS under solar light where the UV fraction of solar light can be utilized for driving the photochemical reaction and the higher wavelength fractions for heating up the suspension. The main purposes of performing this experiment with elevated temperatures are to (i) test whether PFOS photochemical degradation and defluorination can be significantly enhanced at higher temperatures and (ii) shed light on the mechanistic aspect of the photochemical degradation process. As seen in Figure 6 (a) and Table 1, both $k_{obs,PFOS}$ and the defluorination ratio were only slightly enhanced when reaction temperature was increased from 25 °C to 80 °C (by factor 1.3 in

$k_{obs,PFOS}$). We also observed that the initial PFOS adsorption on zeolite is identical at both temperatures. This is most likely a response to various superimposing effects. Briefly, elevated temperatures in the scale tested do not strongly facilitate the photochemical degradation of PFOS. Such results are in accordance with the photon efficiency of the excitation of the PFOS-$Fe^{3+}$ complex as the rate-limiting factor for the photochemical degradation of PFOS.

**3.5. Real water test.** We have demonstrated a successful and efficient photochemical PFOS degradation by UV-C irradiation after adsorption on Fe-doped zeolites in simple reactors. However, for complex matrices of water containing PFOS, like real ground and surface waters, the degradation behavior of PFOS is unknown and thus worthy of investigation. In this study, a groundwater sample was taken from a well located in Leuna, Germany, for testing. Leuna is a former refinery site near Merseburg in the eastern part of Germany. The groundwater sample contains 9.2 nM of PFOS. In addition, other organic compounds, e.g., methyl *tert*-butyl ether (1.9 mg $L^{-1}$) and benzene (3.5 mg $L^{-1}$), were detected in the sample. The detailed chemical composition is presented in Table S3. Due to the very low PFOS concentration in the groundwater sample, preconcentration by zeolite adsorption as described in the SI was performed prior to the reaction. The initial total concentration of PFOS in the zeolite suspension was 46 nM after preconcentration. For comparison, a synthetic water sample with the same PFOS concentration (46 nM) was prepared. Apart from the decreased $k_{obs,PFOS}$ caused by the lower PFOS concentration as discussed in the previous section, the results in Figure 6 (b) and Table 1 show that the degradation performance of PFOS in the groundwater sample is comparable to that in the synthetic water sample with the identical initial PFOS concentration or even slightly better. Nevertheless, a further preconcentration of PFOS concentration is feasible for the improvement of the degradation behavior. Our previous study about the effect of inorganic ions on PFOA photochemical

degradation indicates that sulfate may interfere with the complexation between PFOA and ferric ions and thus reducing the reaction rate.[23] Such an inhibiting effect was not observed in the groundwater sample even though inorganic ions including sulfate were present ($C_{SO_4^{2-}}$ = 5.6 mM). Overall, a certain PFOS enrichment by Fe-BEA35 from a groundwater sample was achieved, and the photochemical PFOS degradation process established seems applicable to a real water matrix.

**3.6. Reusability Test.** From the perspective of practical applications, catalyst stability and reusability are important issues that must be considered. The stability test of Fe-zeolites was evaluated by degrading PFOS in a recycling experimental setup as described in the SI. As shown in Figure S10, the catalyst activity showed a slightly decreasing tendency, but around 90% of its initial activity was maintained with respect to the remaining PFOS percentage in the fourth consecutive run. Two reasons are plausible for the observed decrease in the catalytic performance: (i) hardly avoidable mass losses of the catalyst particles during the reusability test and (ii) a certain carryover of adsorbed PFOS as well as its degradation products during the runs. Nevertheless, the inherent catalyst activity will not be affected for either of these two reasons. The results of the recycling test demonstrate the good stability of Fe-BEA35 and the potential for application.

**3.7. Considerations of Energy Demand.** In terms of practical application, energy demand is an important issue that must be considered. The specific energy consumption (SEC) for 90% PFOS degradation in contaminated water without an enrichment step was calculated to be 468 kWh $m^{-3}$ based on the fluence rate of the photochemical reactor with a 1.1 cm optical path length.[30] Comparing our system with other PFOS *degradation* processes, e.g., the BDD-based electrochemical system, the SEC for 90% PFOS degradation was reported as 20 kWh $m^{-3}$.[31] Apparently, the Fe-zeolite-based photocatalytic system is a highly energy demanding PFOS treatment method. However, thanks to Fe-zeolites' high adsorption affinity toward PFOS, most

water can be discharged after desired PFOS depletion. In such a two-step system, the contribution of SEC for the photocatalytic PFOS destruction as the main driver for energy consumption would be much lower (approximately 47 or 4.7 kWh $m^{-3}$ treated water by assuming a 90 or 99% water disposal). Nevertheless, this energy demand alone corresponds to a contribution of ≥ 1 €/m³, to total operation costs. For the currently prevailing large-scale PFAS *removal* technologies, i.e. activated carbon adsorption, ion exchange and reverse osmosis, full operation treatment costs in the range of 0.5 – 0.9 € $m^{-3}$, 0.8 – 1.7 € $m^{-3}$ and 1.7 – 2.2 € $m^{-3}$ were reported for the example of groundwater pump-and-treat units.[32] This comparison illustrates that further material and process optimization is required for the Fe-zeolite-based photocatalysis system in order to improve energy efficiency and expected operation costs. The present study should be understood as a proof-of-principle for a combined adsorption/photocatalysis approach that not only removes PFAS from water but facilitates their on-site destruction and adsorbent regeneration. More detailed discussion about energy demand and practical application can be found in the SI.

**3.8. Possible Pathways of Photochemical Degradation of PFOS.** Several reaction pathways of photochemical degradation of PFOS have been investigated in the literature.[21, 23, 33-36] Based on the literature study and our experimental results, a possible reaction mechanism is proposed in Scheme 1. First, PFOS is specifically adsorbed on $Fe^{3+}$ sites, forming PFOS-$Fe^{3+}$ complexes (eq 7). After the excitation under UV irradiation, the $Fe^{3+}$ complexes are oxidized via a sulfonate-to-metal electron transfer process to produce $C_8F_{17}SO_3\cdot$ (eq. 8).[21] A similar electron transfer step is proposed in ferric ion mediated photodecomposition and electrochemical oxidation of PFOS in previous studies.[21, 37] The loss of one electron leads to a stretching of the C-S bond, thus easing the desulfurization when reacting with water, yielding perfluorinated alkyl radicals ($\bullet C_8F_{17}$) and sulfate anions (eq 10).

$$C_8F_{17}SO_3\cdot + H_2O \longrightarrow C_8F_{17}\cdot + SO_4^{2-} + 2H^+ \quad (10)$$

The fate of the $\bullet C_8F_{17}$ radical is determined by a number of radical reactions and hydrolysis steps, further detailed in the SI. They are the same for PFOS and PFOA decomposition, regardless of the initial headgroup. In addition, the reduced iron sites ($Fe^{2+}$) will be reoxidized by oxygen or hydroxyl radicals in order to close the photocatalytic cycle (eq 11 and 12). Hydroxyl radicals may be formed during the photolysis of water and ferric species under UV irradiation (eq 13).[38]

$$Fe^{2+}\text{-zeolite} + O_2 \longrightarrow Fe^{3+}\text{-zeolite} + \cdot O_2^- \quad (11)$$

$$Fe^{2+}\text{-zeolite} + \cdot OH \longrightarrow Fe^{3+}\text{-zeolite} + OH^- \quad (12)$$

$$Fe^{3+}\text{-zeolite} + H_2O \xrightarrow{UV} Fe^{2+}\text{-zeolite} + \cdot OH + H^+ \quad (13)$$

## 4. ENVIRONMENTAL IMPLICATIONS.

The idea of using Fe-zeolites as both adsorbent and photocatalyst enables an efficient technological approach for PFOS removal and degradation as well as on-site sorbent regeneration. In the first step, PFOS is removed from the large volume of incoming water by adsorption onto the Fe-zeolites, which can be separated, e.g., by filtration. In the second step, the concentrate of the loaded zeolite particles can be regenerated *in situ* by photochemical degradation with UV-C irradiation. The resulting byproducts, i.e., short-chain PFCAs, are desorbed into the aqueous phase. Their complete mineralization can be achieved in the regeneration solution (third step) by combination with UV activation of sodium persulfate. The Fe-zeolite, as a separable adsorbent, is able to catalyze not only PFOS but also PFOA degradation in the adsorbed state. Thus, our findings are relevant for the following: (i) the development of adsorptive PFAS removal technologies combined with on-site adsorbent regeneration; (ii) inspiring PFAS removal approaches based on

other Fe-loaded catalysts; and (iii) providing suggestions for future studies on material optimization, reactor, and process design.

**Supporting Information**

Additional tables, figures, discussions, and detailed experimental procedures on gas phase product analysis, adsorption degree of PFCAs on zeolite, full mineralization of short-chain intermediates and reusability test.

**Corresponding Author**

(A. Georgi) E-mail address: anett.georgi@ufz.de

**ACKNOWLEDGMENTS**

We thank Jieying Zhou for useful discussions and proofreading. L.Q. acknowledges financial support from China Scholarship Council.

**Table 1**. Adsorption and Kinetic Data on PFOS Degradation with Varying Initial PFOS and Zeolite Concentrations [f]

| | **0.25 g L$^{-1}$ zeolite 10 μM PFOS** | **0.5 g L$^{-1}$ zeolite 20 μM PFOS** | **1.0 g L$^{-1}$ zeolite 40 μM PFOS** | **0.5 g L$^{-1}$ zeolite 10 μM PFOS** | **0.5 g L$^{-1}$ zeolite 0.046 μM PFOS** | **0.5 g L$^{-1}$ zeolite 0.046 μM PFOS in real water** | **0.5 g L$^{-1}$ zeolite 20 μM PFOS at 80 °C** |
|---|---|---|---|---|---|---|---|
| **$X_{sorb,\ PFOS}$ (%)** | 96.6 | 98.6 | 99.2 | 98.9 | 99.6 | 99.5 | 98.8 |
| **$C_{PFOS,free}$ (μM)** | 0.34 | 0.28 | 0.33 | 0.11 | 0.00019 | 0.00025 | 0.25 |
| **$q_{PFOS}$ (wt%) [a]** | 1.92 | 1.96 | 1.98 | 0.99 | 0.0046 | 0.0046 | 1.96 |
| **$K_d$ (L kg$^{-1}$) [b]** | $11\times10^4$ | $14\times10^4$ | $12\times10^4$ | $19\times10^4$ | $47\times10^4$ | $36\times10^4$ | $15\times10^4$ |
| **$d_{F^-}$ after 96 h (%)** | 60 | 69 | 70 | 66 | - [c] | - | 72 |
| **$k_{obs,PFOS}$ (h$^{-1}$)** | 0.067±0.013[d] | 0.10±0.02 | 0.13±0.02 | 0.095±0.024 | 0.013±0.002 | 0.020±0.002 | 0.13±0.05 |
| **PFOS $t_{1/2}$ (h)** | 10±2 | 7±1 | 5±1 | 7±1 | 54±6 | 34±5 | 5±1 |

[f] At $pH_0$=3.0, oxygen atmosphere, T = 25°C if not otherwise noted.

[a] Sorbent loading.

[b] Single point adsorption coefficient $K_d$ (L kg$^{-1}$) = $q_{PFOS}$ (μmol kg$^{-1}$)/$C_{PFOS,free}$ (μmol L$^{-1}$).

[c] Not available.

[d] The error ranges are derived from the regression analysis of the data.

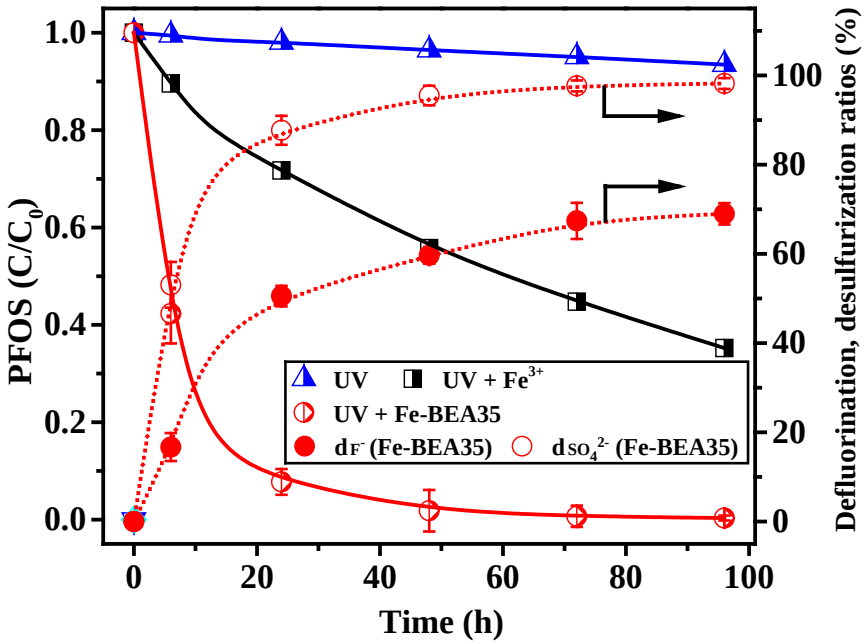


**Figure 1**. Comparison of PFOS degradation and product formation in three experiments: (i) UV alone, (ii) UV and ferric ions, and (iii) UV and Fe-BEA35. $C_{0,PFOS}$ = 20 μM, $pH_0$ = 3.0, oxygen atmosphere, 0.5 g $L^{-1}$ Fe-BEA35 (1.3 wt% Fe in zeolites), and $C_{0,Fe^{3+}}$ = 200 μM, where applied. Error ranges stand for the standard deviations of the results from triplicate assays. Lines serve as guides for the eye.

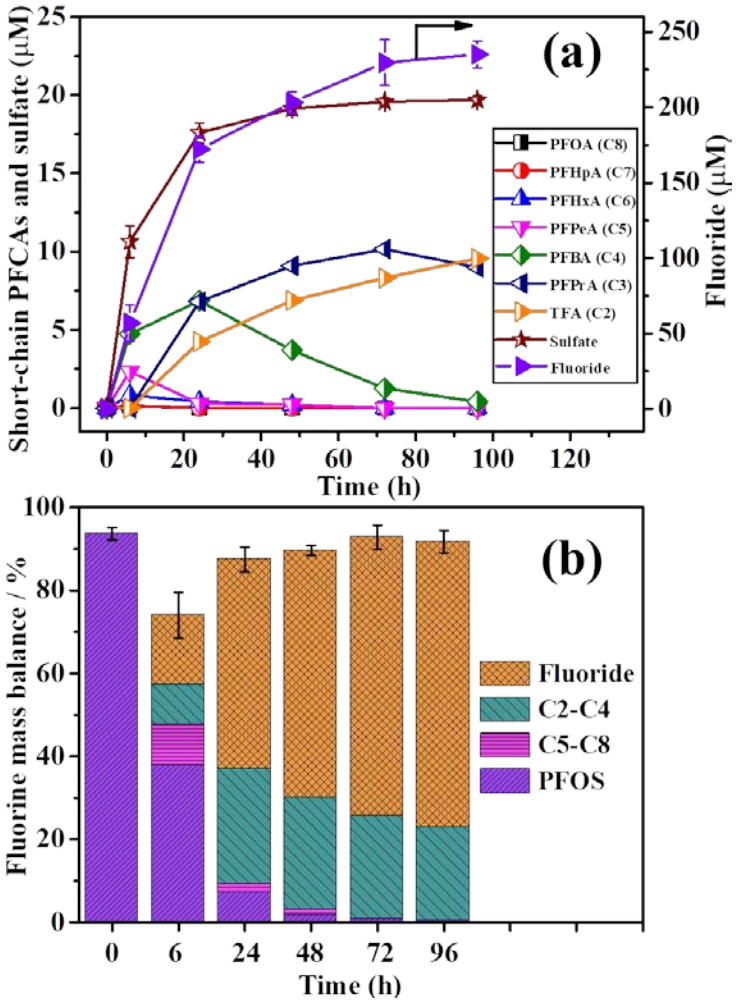


**Figure 2**. (a) Formation of short-chain PFCA intermediates, fluoride and sulfate during photochemical degradation of PFOS and (b) fluorine mass balance during photochemical degradation of PFOS. The 0-h mass balance represents fluorine detected as PFOS in zeolite suspension by ACN extraction before the start of irradiation. The 96-h mass balance represents fluorine detected as fluoride and C2 to C4 PFCAs in aqueous phase and C5 to C8 PFCAs and PFOS by ACN extraction. 0.5 g $L^{-1}$ Fe-BEA35, $C_{0,PFOS}$ = 20 μM, $pH_0$ = 3.0, oxygen atmosphere. Error ranges stand for the standard deviations of the results from triplicate assays in Figure 2(a). The cumulative error is shown in Figure 1 (b). Lines serve as guides for the eye.

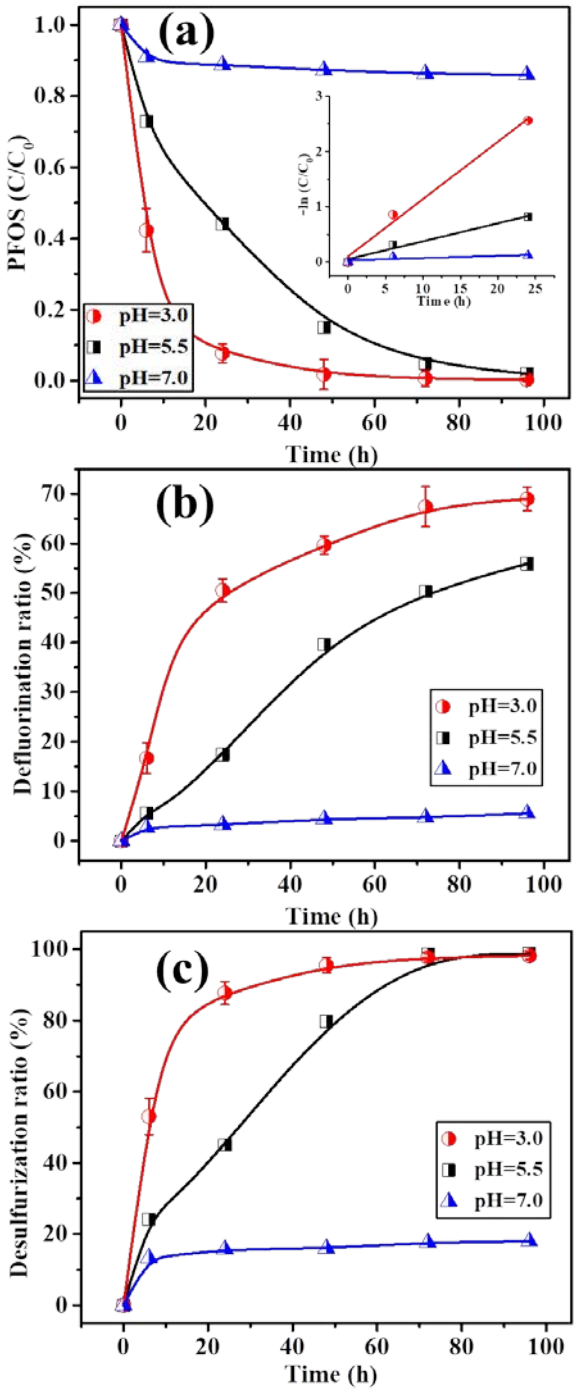


**Figure 3**. Degradation of PFOS under UV-C irradiation at various initial pH values. Time course of (a) residual PFOS concentration; (b) defluorination ratios ($d_{F^-}$), and (c) desulfurization ratios ($d_{SO_4^{2-}}$). 0.5 g $L^{-1}$ Fe-BEA35, $C_{0,PFOS}$ = 20 μM, oxygen atmosphere. Error ranges stand for the standard deviations of the results from triplicate assays. Lines serve as guides for the eye.

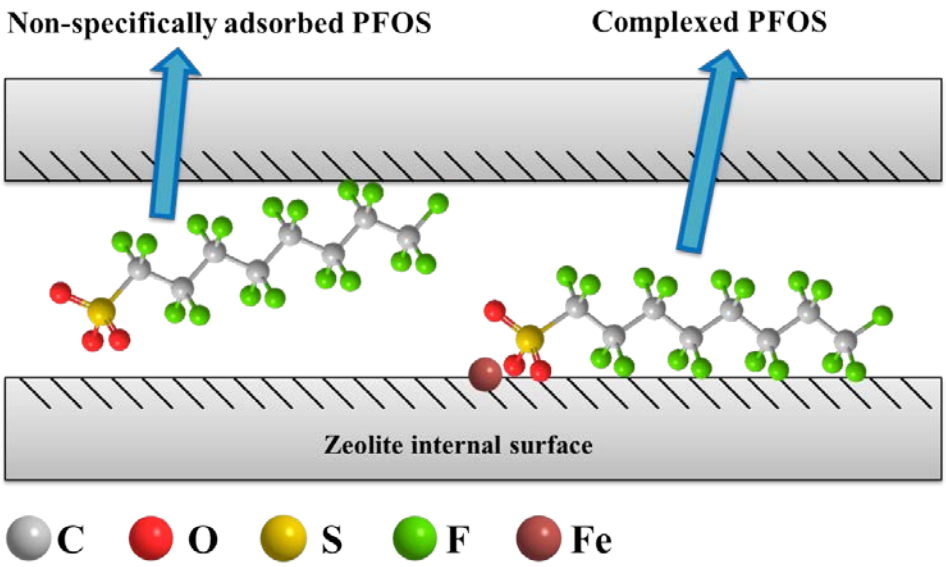


**Figure 4.** Schematic diagram of PFOS configurations on Fe-BEA35 with and without specific adsorption. The term "complexed PFOS" means the specifically adsorbed PFOS at ferric ions.

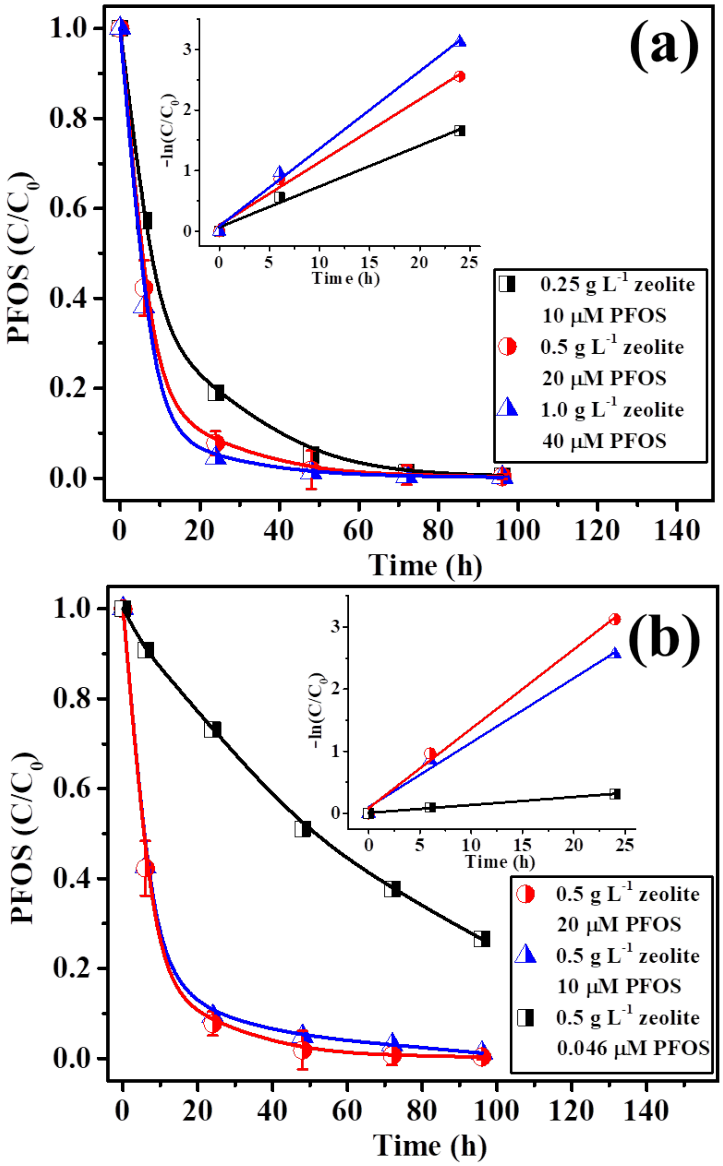


**Figure 5**. Degradation of PFOS under UV-C irradiation: (a) in the presence of various zeolite dosages and (b) with various initial PFOS concentrations. $pH_0$ = 3.0, oxygen atmosphere. Error ranges stand for the standard deviations of the results from triplicate assays. Lines serve as guides for the eye.

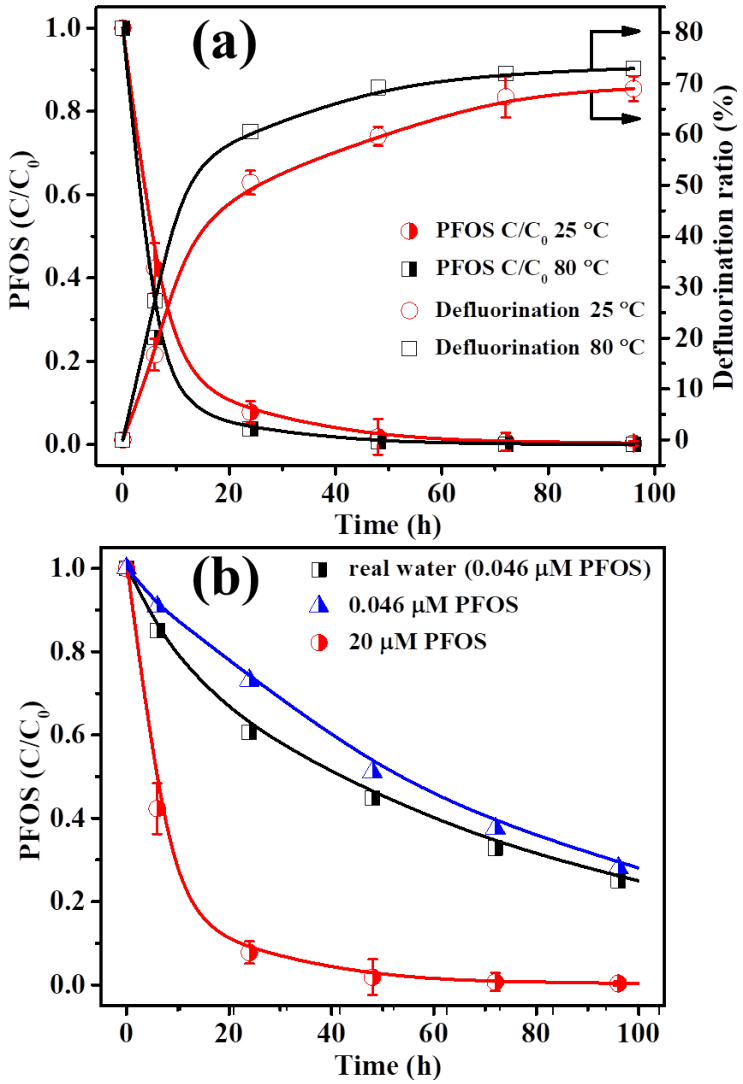


**Figure 6**. Degradation of PFOS under UV-C irradiation: (a) at different operation temperatures, $C_{0,PFOS}$ = 20 μM and (b) in a real groundwater sample and synthetic water samples with various initial PFOS concentrations. 0.5 g $L^{-1}$ Fe-BEA35, $pH_0$ = 3.0, oxygen atmosphere. Error ranges stand for the standard deviations of the results from triplicate assays. Lines serve as guides for the eye.

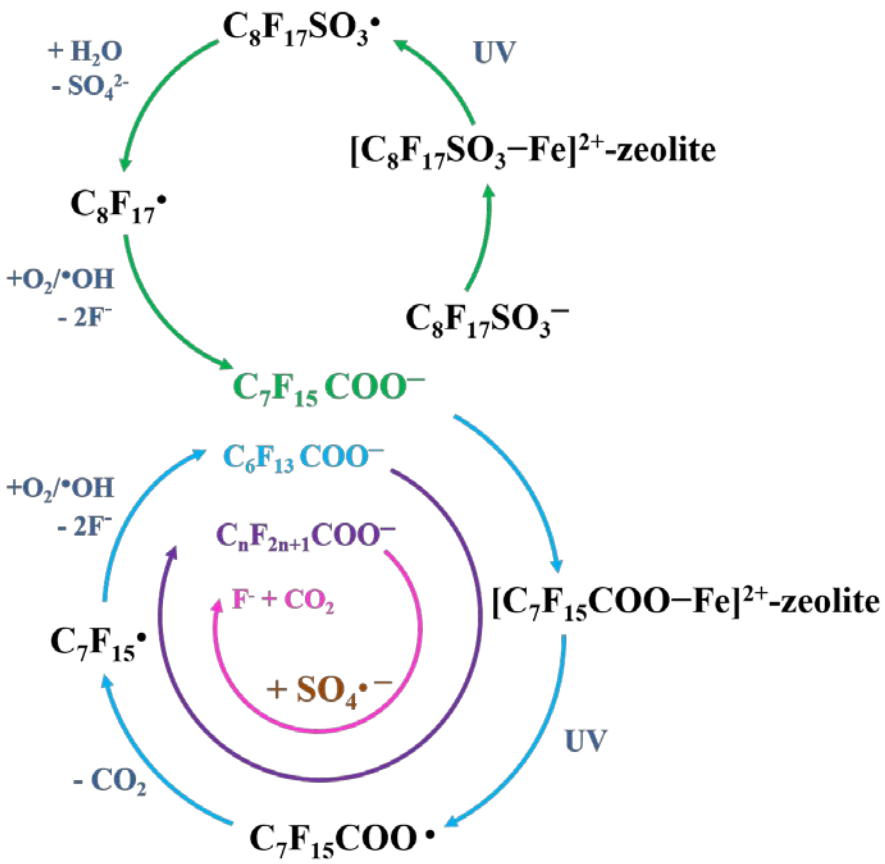


**Scheme 1**. Proposed reaction mechanism for PFOS photochemical degradation on Fe-BEA35. Detailed radical reactions and hydrolysis steps are presented in SI.

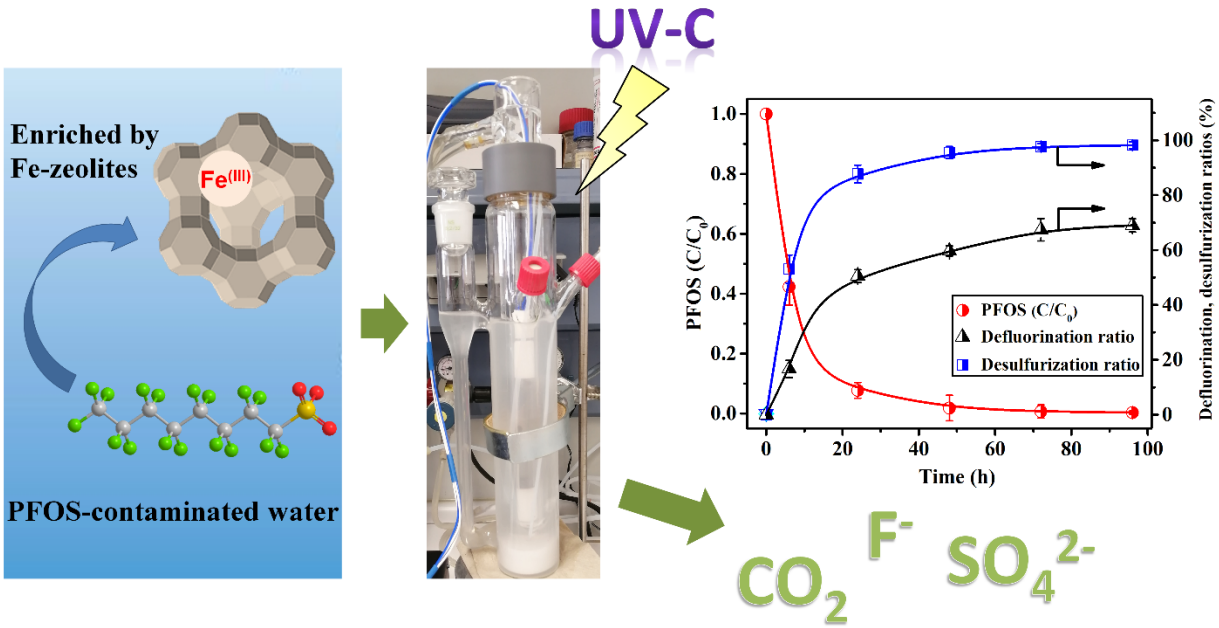
UV-C
Enriched by
Fe-zeolites
Fe(III)
PFOS-contaminated water
PFOS (C/C0)
Defluorination ratio
Desulfurization ratio
Time (h)
Defluorination, desulfurization ratios (%)
CO2
F-
SO42-

**TOC graphic**

## REFERENCES


1. Pistocchi, A.; Loos, R., A map of European emissions and concentrations of PFOS and PFOA. *Environ. Sci. Technol.* **2009,** *43*, (24), 9237-9244.

2. Arrieta-Cortes, R.; Farias, P.; Hoyo-Vadillo, C.; Kleiche-Dray, M., Carcinogenic risk of emerging persistent organic pollutant perfluorooctane sulfonate (PFOS): A proposal of classification. *Regul. Toxicol. Pharmacol.* **2017,** *83*, 66-80.

3. Ahrens, L.; Xie, Z.; Ebinghaus, R., Distribution of perfluoroalkyl compounds in seawater from Northern Europe, Atlantic Ocean, and Southern Ocean. *Chemosphere* **2010,** *78*, (8), 1011-1016.

4. Eriksson, U.; Roos, A.; Lind, Y.; Hope, K.; Ekblad, A.; Kärrman, A., Comparison of PFASs contamination in the freshwater and terrestrial environments by analysis of eggs from osprey (Pandion haliaetus), tawny owl (Strix aluco), and common kestrel (Falco tinnunculus). *Environ. Res.* **2016,** *149*, 40-47.

5. González-Doncel, M.; Fernández Torija, C.; Pablos, M. V.; García Hortigüela, P.; López Arévalo, M.; Beltrán, E. M., The role of PFOS on triclosan toxicity to two model freshwater organisms. *Environ. Pollut.* **2020,** *263*, 114604.

6. Eriksen, K. T.; Raaschou-Nielsen, O.; Sørensen, M.; Roursgaard, M.; Loft, S.; Møller, P., Genotoxic potential of the perfluorinated chemicals PFOA, PFOS, PFBS, PFNA and PFHxA in human HepG2 cells. *Mutat. Res.-Gen. Tox. En.* **2010,** *700*, (1-2), 39-43.

7. Harada, K.; Xu, F.; Ono, K.; Iijima, T.; Koizumi, A., Effects of PFOS and PFOA on L-type Ca2+ currents in guinea-pig ventricular myocytes. *Biochem. Biophys. Res.* **2005,** *329*, (2), 487-494.

8. Fei, C.; McLaughlin, J. K.; Lipworth, L.; Olsen, J., Maternal levels of perfluorinated chemicals and subfecundity. *Hum. Reprod.* **2009,** *24*, (5), 1200-1205.

9. Johansson, N.; Fredriksson, A.; Eriksson, P., Neonatal exposure to perfluorooctane sulfonate (PFOS) and perfluorooctanoic acid (PFOA) causes neurobehavioural defects in adult mice. *Neurotoxicology* **2008,** *29*, (1), 160-169.

10. Sunderland, E. M.; Hu, X. C.; Dassuncao, C.; Tokranov, A. K.; Wagner, C. C.; Allen, J. G., A review of the pathways of human exposure to poly- and perfluoroalkyl substances (PFASs) and present understanding of health effects. *J. Exposure Sci. Environ. Epidemiol.* **2019,** *29*, (2), 131-147.

11. Sekiguchi, K.; Kudo, T.; Sankoda, K., Combined sonochemical and short-wavelength UV degradation of hydrophobic perfluorinated compounds. *Ultrason. Sonochem.* **2017,** *39*, 87-92.

12. Javed, H.; Lyu, C.; Sun, R.; Zhang, D.; Alvarez, P. J. J., Discerning the inefficacy of hydroxyl radicals during perfluorooctanoic acid degradation. *Chemosphere* **2020,** *247*, 125883.

13. Trojanowicz, M.; Bojanowska-Czajka, A.; Bartosiewicz, I.; Kulisa, K., Advanced Oxidation/Reduction Processes treatment for aqueous perfluorooctanoate (PFOA) and perfluorooctanesulfonate (PFOS) – A review of recent advances. *Chem. Eng. J.* **2018,** *336*, 170-199.

14. Bruton, T. A.; Sedlak, D. L., Treatment of perfluoroalkyl acids by heat-activated persulfate under conditions representative of in situ chemical oxidation. *Chemosphere* **2018,** *206*, 457-464.

15. Park, H.; Vecitis, C. D.; Cheng, J.; Dalleska, N. F.; Mader, B. T.; Hoffmann, M. R., Reductive degradation of perfluoroalkyl compounds with aquated electrons generated from iodide photolysis at 254 nm. *Photochem. Photobiol. Sci.* **2011,** *10*, (12), 1945-1953.

16. Bentel, M. J.; Yu, Y.; Xu, L.; Li, Z.; Wong, B. M.; Men, Y.; Liu, J., Defluorination of per- and polyfluoroalkyl substances (PFASs) with hydrated electrons: Structural dependence and implications to PFAS remediation and management. *Environ. Sci. Technol.* **2019,** *53*, (7), 3718-3728.

17. Tian, H.; Gao, J.; Li, H.; Boyd, S. A.; Gu, C., Complete defluorination of perfluorinated compounds by hydrated electrons generated from 3-indole-acetic-acid in organomodified Montmorillonite. *Sci. Rep.* **2016,** *6*, (1), 32949.

18. Carter, K. E.; Farrell, J., Oxidative destruction of perfluorooctane sulfonate using boron-doped diamond film electrodes. *Environ. Sci. Technol.* **2008,** *42*, (16), 6111-6115.

19. Grčić, I.; Li Puma, G., Photocatalytic degradation of water contaminants in multiple photoreactors and evaluation of reaction kinetic constants independent of photon absorption, irradiance, reactor geometry, and hydrodynamics. *Environ. Sci. Technol.* **2013,** *47*, (23), 13702-13711.

20. Sun, Z.; Zhang, C.; Chen, P.; Zhou, Q.; Hoffmann, M. R., Impact of humic acid on the photoreductive degradation of perfluorooctane sulfonate (PFOS) by UV/iodide process. *Water Res.* **2017,** *127*, 50-58.

21. Jin, L.; Zhang, P.; Shao, T.; Zhao, S., Ferric ion mediated photodecomposition of aqueous perfluorooctane sulfonate (PFOS) under UV irradiation and its mechanism. *J. Hazard. Mater.* **2014,** *271*, 9-15.

22. Liang, X.; Cheng, J.; Yang, C.; Yang, S., Factors influencing aqueous perfluorooctanoic acid (PFOA) photodecomposition by VUV irradiation in the presence of ferric ions. *Chem. Eng. J.* **2016,** *298*, 291-299.

23. Qian, L.; Georgi, A.; Gonzalez-Olmos, R.; Kopinke, F.-D., Degradation of perfluorooctanoic acid adsorbed on Fe-zeolites with molecular oxygen as oxidant under UV-A irradiation. *Appl. Cat. B: Environ.* **2020,** *278*, 119283.

24. Brooke, D.; Footitt, A.; Nwaogu, T. *Environmental risk evaluation report: Perfluorooctanesulphonate (PFOS)*; Environment Agency, UK, 2004.

25. Shafique, U.; Dorn, V.; Paschke, A.; Schuurmann, G., Adsorption of perfluorocarboxylic acids at the silica surface. *Chem. Commun.* **2017,** *53*, (3), 589-592.

26. Punyapalakul, P.; Suksomboon, K.; Prarat, P.; Khaodhiar, S., Effects of surface functional groups and porous structures on adsorption and recovery of perfluorinated compounds by inorganic porous silicas. *Sep. Sci. Technol.* **2013,** *48*, (5), 775-788.

27. Ochoa-Herrera, V.; Sierra-Alvarez, R., Removal of perfluorinated surfactants by sorption onto granular activated carbon, zeolite and sludge. *Chemosphere* **2008,** *72*, (10), 1588-1593.

28. Hogfeldt, E., *Stability constants of metal-ion complexes. Part A Inorganic ligands. International Union of Pure and Applied Chemists.* Pergamon Press: New York, 1982.

29. Tang, B.; Yu, L.; Huang, S.; Luo, J.; Zhuo, Y., Energy efficiency of pre-treating excess sewage sludge with microwave irradiation. *Bioresour. Technol.* **2010,** *101*, (14), 5092-5097.

30. Katsoyiannis, I. A.; Canonica, S.; von Gunten, U., Efficiency and energy requirements for the transformation of organic micropollutants by ozone, $O_3/H_2O_2$ and $UV/H_2O_2$. *Water Res.* **2011,** *45*, (13), 3811-3822.

31. Wang, L.; Lu, J.; Li, L.; Wang, Y.; Huang, Q., Effects of chloride on electrochemical degradation of perfluorooctanesulfonate by Magnéli phase Ti4O7 and boron doped diamond anodes. *Water Res.* **2020,** *170*, 115254.

32. *Züblin Umwelttechnik GmbH* Website; https://www.zueblin-umwelttechnik.com/

33. Wang, S.; Yang, Q.; Chen, F.; Sun, J.; Luo, K.; Yao, F.; Wang, X.; Wang, D.; Li, X.; Zeng, G., Photocatalytic degradation of perfluorooctanoic acid and perfluorooctane sulfonate in water: A critical review. *Chem. Eng. J.* **2017,** *328*, 927-942.

34. Hori, H.; Yamamoto, A.; Koike, K.; Kutsuna, S.; Osaka, I.; Arakawa, R., Photochemical decomposition of environmentally persistent short-chain perfluorocarboxylic acids in water mediated by iron (II)/(III) redox reactions. *Chemosphere* **2007,** *68*, (3), 572-578.

35. Lutze, H. V.; Brekenfeld, J.; Naumov, S.; von Sonntag, C.; Schmidt, T. C., Degradation of perfluorinated compounds by sulfate radicals–New mechanistic aspects and economical considerations. *Water Res.* **2018,** *129*, 509-519.

36. Liu, D.; Xiu, Z.; Liu, F.; Wu, G.; Adamson, D.; Newell, C.; Vikesland, P.; Tsai, A.-L.; Alvarez, P. J., Perfluorooctanoic acid degradation in the presence of Fe(III) under natural sunlight. *J. Hazard. Mater.* **2013,** *262*, 456-463.

37. Zhuo, Q.; Luo, M.; Guo, Q.; Yu, G.; Deng, S.; Xu, Z.; Yang, B.; Liang, X., Electrochemical oxidation of environmentally persistent perfluorooctane sulfonate by a novel lead dioxide anode. *Electrochim. Acta* **2016,** *213*, 358-367.

38. Benkelberg, H.-J.; Warneck, P., Photodecomposition of iron(III) hydroxo and sulfato complexes in aqueous solution: wavelength dependence of OH and $SO_4^-$ quantum yields. *J. Phys. Chem.* **1995,** *99*, (14), 5214-5221.